# Ordered Structure in Block Polymer Solutions. 5. Equilibrium and Nonequilibrium Aspects of Microdomain Formation

**Mitsuhiro Shibayama, Takeji Hashimoto,* and Hiromichi Kawai**

*Department of Polymer Chemistry, Faculty of Engineering, Kyoto University, Kyoto 606, Japan.* *Received October 12, 1982*

ABSTRACT: Equilibrium and nonequilibrium aspects of the microdomain formation of AB-type diblock polymers in neutral solvents were studied by investigating the domain size as a function of polymer volume concentration $\phi_P$ and temperature $T$ by means of the small-angle X-ray scattering technique. It was shown that there are two regimes in the concentration and temperature dependence of the domain size: (i) the *equilibrium regime*, where the size is *thermodynamically controlled*—i.e., the greater the segregation power between A and B (i.e., the higher the value $\phi_P$ or the lower the value $T$), the larger the size—and (ii) the *nonequilibrium regime*, where the size is *kinetically controlled*. In the latter regime, for a given time scale of experiments, the average distance $a$ between the neighboring chemical junction points along the interface or the average number of block chains $N$ per spherical domain cannot follow equilibrium but is fixed more or less to a constant value. Consequently, in this regime the size decreases with increasing $\phi_P$ and decreasing $T$ simply due to the effects of *deswelling* and *thermal contraction*, respectively. The crossover between the two regimes (at $T = T_f$ or $\phi_P = \phi_f$) was found to depend on morphology: the lamellar microdomains have a higher concentration $\phi_f$ than the spherical microdomains, and hence the former domain systems are closer to equilibrium than the latter domain systems. This difference in the crossover points $T_f$ and $\phi_f$ and molecular-weight dependence of the crossover points are discussed in terms of two kinds of potential barriers for the growth of the domains, i.e., for changing the value $a$ or $N$: (i) the barrier associated with the frictional interactions accompanied by the translational diffusion of chemical junction points of block polymers along the interface (frictional potential barrier) and (ii) the barrier associated with the thermodynamic interactions accompanied by mixing of a given block chain (e.g., A) with unlike chains (e.g., B) (*thermodynamic potential barrier*). The latter potential is unique to and dominant for the growth of the spherical microdomains but is less significant for the growth of the lamellar microdomains.

## Introduction

If A and B polymers in AB diblock or ABA triblock polymers have different cohesive energy densities, they tend to phase separate in the segregation limit where $\chi Z$ is greater than a critical value[1-7] ($\chi$ being the Flory–Huggins interaction parameter between the A and B segments and $Z$ being the total degree of polymerization of the block polymers). However, this phase segragation cannot be extended to macroscopic spatial scale but is limited to molecular dimensions owing to the molecular constraint of A and B being covalently bonded. This is the so-called *microphase separation* and gives rise to five fundamental microdomain structures depending on fractional composition of the block polymers: A spheres in a B matrix, A cylinders in a B matrix, alternating lamellae of A and B, and the phase-inverted structures of the first two structures. The radii of the spheres and cylinders and the thicknesses of the lamellae as well as their interdomain distances are related to the molecular dimensions of the A and B polymer chains.

The equilibrium domain morphology is the one that minimizes the free energy of the microdomain. The equilibrium theories[3,4,8,9] predict that the domain size and the interdomain distance are functions of fundamental molecular parameters such as $Z_A$ and $Z_B$ (degrees of polymerization of the A and B chains), $\chi$, the Kuhn statistical segment lengths $b_A$ and $b_B$, and the segment densities $\rho_{0A}$ and $\rho_{0B}$ of pure bulk A and B polymers. Since all these parameters are measurable quantities, one can compare the experimental and theoretical domain sizes and interdomain distances. In one of our earlier papers we presented comparisons between the measured and calculated domain size for the lamellar microdomains (see Figure 1)[10] and for the spherical microdomains (see Figure 2).[11]

Figure 1 shows the comparison between the calculated and measure lamellar identity period $D$ as a function of total molecular weight of diblock polymers $M_n$. Figure 1 is a revised version of Figure 12 of our previous paper,[10] to which we added the data recently reported by Hadzioannou and Skoulios (HS)[26] (data marked by open squares). The references for the works cited in the figure (other than HS) were given in the paper of ref 10 and will not be repeated here. The triblock polymers S–B–S were treated as the diblock polymers of S–$^1/_2$B. The solid line indicates calculated results from the theories of Helfand and Wasserman (HW)[3] and Meier (M)[9] for diblock polymers having equal block molecular weights with the parameters described in the previous paper.[10] It should be noted that the two theoretical results HW and M are degenerate in this ordinate scale. Although there is some scattering in the data points measured by a number of groups for a number of di- and triblock polymers, owing to the differences in the chemical composition and microstructure for each polymer as well as those in the film preparation processes, good agreement was obtained between the experimental and calculated $D$. We have recently obtained a good agreement between the calculated and measured results also for a series of block polymers having cylindrical microdomains.[20] The data obtained by Richards and Thomason[27] also seem to indicate a good or moderate agreement between the theoretical and experimental values for the lamellar and cylindrical microdomains. Thus the lamellar and cylindrical microdomain systems are predictable essentially by the equilibrium theories and, therefore, from fundamental molecular parameters such as $Z_K$, $\rho_{0K}$, $b_K$, and $\chi$.

Figure 2 shows the measured and calculated $R_s$ (radius of sphere) and $D_s$ (intersphere distance)[22] as a function of molecular weight of the block chains forming the spheres, $(M_n)_{sphere}$, and total molecular weight of the block polymer, $(M_n)_{total}$. The figure is a revised version of Figure 12 of ref 11, to which we added the data corrected for the nonequilibrium effect as will be shown later in the text (the data marked by the diamond-shaped arrows). The solid lines are calculated from the theory of Helfand and Wasserman (HW)[3] for diblock polymers having 20 wt % polyisoprene or polybutadiene. Polybutadiene was assumed to have the same parameters as those for polyisoprene. The triblock

0024-9297/83/2216-1434$01.50/0 

Table I
Block Polymers Used in This Work

| specimen code | type of block polymer[a] | wt % PS | total $M_n \times 10^{-4}$ [b] | morphology in bulk[c] |
|---|---|---|---|---|
| S-4 | S-I | 85 | 22 | PI spheres in a PS matrix |
| L-8 | S-I | 50 | 9.4 | alternating lamellae |
| SB | S-B | 82.5 | 9.2 | PB spheres in a PS matrix |

[a] S-I designates polystyrene-polyisoprene diblock polymers. [b] Number-average molecular weight. [c] PI, PS, and PB designate, respectively, polyisoprene, polystyrene, and polybutadiene block chains.

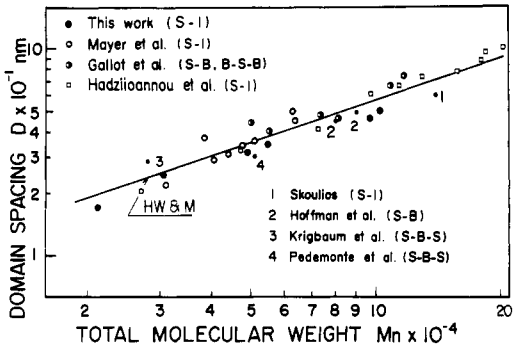


**Figure 1.** Comparison between measured and calculated average domain spacings $D$ as a function of total molecular weight of block polymers $M_n$. Calculated results (solid line) were obtained from the theories of Meier (M) and Helfand and Wasserman (HW) for diblock polymers AB having equal molecular weights for A and B. A–B–A polymers were treated as the diblock polymers of A–$^1/_2$B (based on Hashimoto et al.[10]).

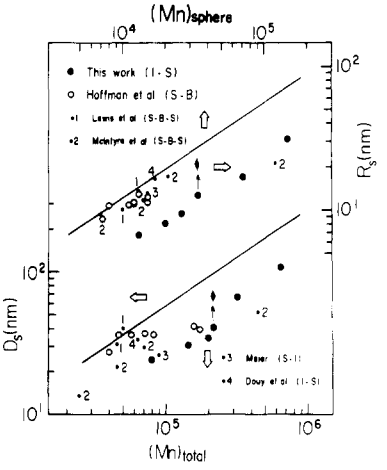


**Figure 2.** Comparison between measured and calculated radius of sphere $R_s$ and intersphere distance $D_s$. The solid lines are calculated from the theory of Helfand and Wasserman from block polymers having 20 wt % polysioprene or polybutadiene. $(M_n)_{sphere}$ designates the molecular weight of the block chain forming the spherical domain. Solid diamond-shaped arrows indicate the corrected values for the nonequilibrium effect according to the method as described in section IV-2 (based on Hashimoto et al.[11]).

polymers S–B–S were again treated as diblock polymers S–$^1/_2$B. Although the data points are somewhat scattered as in the case of lamellar microdomains, the general trend is that the observed values are generally much smaller than the calculated values. Our data (large solid circles) show that the observed values are much less than the predicted values but that relative molecular weight dependence of the observed values $D_s$ and $R_s$ are in good agreement with the theoretical results. Deviations from the theory have been found also by Richards et al.[27] and Bates et al.[28]

These peculiar phenomena of spherical microdomain systems, in contrast to the lamellar microdomain systems, were qualitatively interpreted based on equilibrium and nonequilibrium aspects in the domain formation.[11] In this paper we further extend our studies along this line by

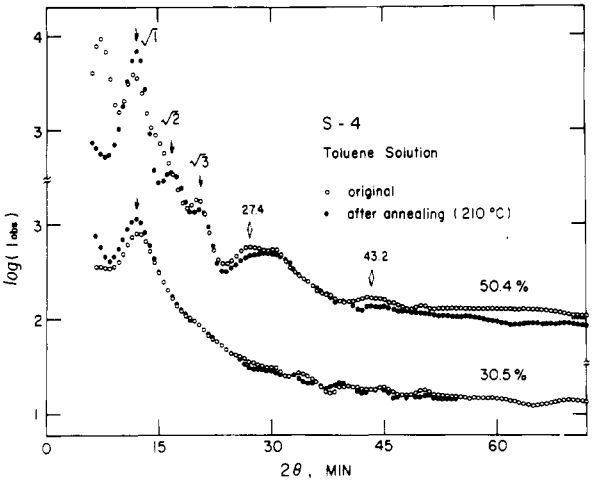


**Figure 3.** Effects of annealing as-prepared toluene solutions of S-4 on the SAXS profiles at room temperature. Thin arrows indicate the scattering maxima arising from interparticle interference and the diamond-shaped arrows indicate the maxima arising from intraparticle interference.

investigating the microdomains as a function of polymer concentration and temperature.

It should be noted that the present studies may also give fundamental information on *physical aging* of such submicroscopic composite systems. The greater the nonequilibrium effect involved in the systems, the larger is the physical aging effect.

## II. Experimental Section

**1. Specimens.** Three kinds of block polymers were prepared by living anionic polymerization. Their characteristics are summarized in Table I.

The block polymer solutions were prepared with two kinds of neutral solvents, toluene and dioctyl phthalate (DOP), which are good for polystyrene (PS), polyisoprene (PI), and polybutadiene (PB). The DOP solutions were prepared by mixing prescribed amounts of the block polymers and the DOP (a fixed oil) with an excess amount of methylene chloride, which was subsequently evaporated completely until the specimens showed a constant weight to obtain a homogeneous solution of a given concentration. The block polymer solutions at a given concentration were then sampled into a scattering cell as described in detail in previous papers,[12,13] and the scattering from the solutions was measured at constant concentration and temperature.

**2. SAXS Measurements.** Small-angle X-ray scattering (SAXS) from the solutions was measured with a rotating-anode X-ray generator (Cu K$\alpha$ radiation, operated at 50 kV and 200 mA) with a position-sensitive linear detector or with a conventional step-scanning X-ray detector as described in detail in our earlier papers.[14-16] Unless otherwise stated, the SAXS data were corrected for absorption, background scattering (air scattering and parasitic scattering, the correction for thermal diffuse scattering being excluded), nonuniformity of the detector sensitivity, and collimation errors in both the slit-width and slit-length directions according to a method as described elsewhere.[15,16]

## III. Results

**1. Spherical Microdomains. (a) Concentration and Temperature Dependence.** Figure 3 shows a typical

example of a nonequilibrium effect on the SAXS profiles of 30.5 and 50.4 wt % toluene solutions of the block polymer S-4. There is no significant change in the profiles before (open circles) and after annealing the solution (solid circles) of lower concentration (e.g., 30.5 wt %) at 210 °C, but a significant change is seen for the solution at higher concentration (e.g., 50.4 wt %). Thus the higher the concentration, the larger the annealing effect, and hence the larger the nonequilibrium effect.

It was found that the first-order scattering maximum at scattering angle $2\theta \simeq 7$ min arc (Cu K$\alpha$ radiation) for the as-prepared solution loses its intensity and disappears with increasing temperature up to 210 °C. It did not recover its intensity when the temperature lowered. The origin of the first-order peak is not well understood at present, but it might be due to concentration fluctuations existing in the as-prepared solutions (the as-prepared solutions being stored at room temperature for at least a few days after the sample was visually solubilized).

The SAXS profiles from the annealed solution with 50.4 wt % polymer concentration exhibits distinct scattering maxima as shown by thin arrows (which arise from interparticle interference) at the scattering angle corresponding to $\sqrt{2}$ and $\sqrt{3}$ times the scattering angle of the first-order maximum at $2\theta = 11.9$ min arc. This profile is typical of that for the system where the spherical microdomains are packed in space in a simple-cubic or body-centered-cubic lattice as discussed in our previous papers.[12] The broad maxima at $2\theta \simeq 27.4$ and 43.2 min arc (marked by diamond-shaped arrows) are the scattering maxima from the isolated spheres, the interference function approaching unity at these large scattering angles.[12]

One can estimate the Bragg spacing $D_s$ from the interparticle interference maxima, e.g., from the peak position of the first-order maximum, $2\theta_m$

$$2D_s \sin \theta_m = \lambda \qquad \text{(III-1)}$$

One can also estimate the average radius of the spheres $R_s$ from the peak positions $2\theta_{m,i}$ of the intraparticle maxima

$$4\pi(R_s/\lambda) \sin \theta_{m,i} = 5.765, \quad i = 1$$
$$= 9.10, \quad i = 2 \qquad \text{(III-2)}$$

At lower concentrations the microdomains have greater lattice disordering, resulting in disappearance of the higher order scattering maxima and in a broader first-order maximum. Moreover, the microdomains have a more diffuse boundary and a thicker interphase, resulting in disappearance of the scattering maxima arising from the isolated spheres. The lattice disordering and the effect of the diffuse boundary on the SAXS profiles will be discussed in more detail in section IV-4.

Figure 4 shows the concentration dependence of the SAXS profiles at room temperature for toluene solutions of S-4. These profiles were obtained for solutions annealed at 210 °C for about 0.5 h. It is clearly seen that the spherical microdomains (in which the solvated polyisoprene spheres are dispersed in the matrix of polystyrene solution) are developed at concentrations between 20.7 and 30.5 wt % polymer. At concentrations greater than 40 wt %, the microdomains have well-developed long-range spatial order, packed in a cubic lattice. The Bragg spacing $D_s$ and the radius $R_s$ are estimated from eq III-1 and III-2 and are plotted as a function of polymer volume concentration $\phi_P$ (see the data shown by solid circles in Figure 5). The values $D_s$ and $R_s$ tend to decrease with increasing $\phi_P$, which is in sharp contrast with the concentration dependence of $D$ in lamellar domains at $\phi_P < \phi_f$ (see Figure 7). The decreases of $D_s$ and $R_s$ with $\phi_P$ are phenomena similar to that found in the lamellar domains at $\phi_P \geq \phi_f$

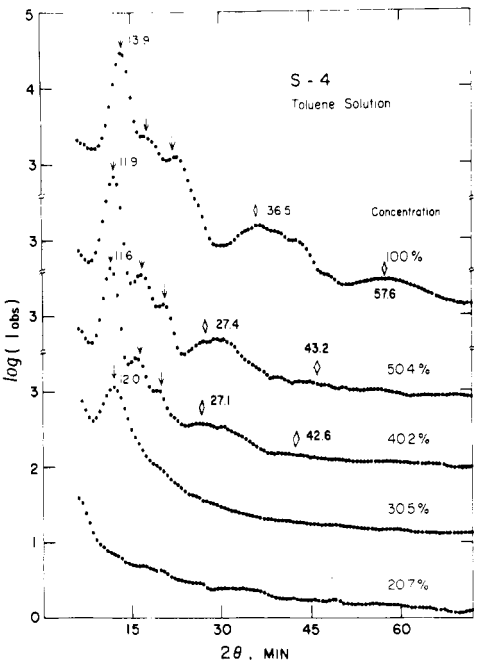


**Figure 4.** SAXS profiles for toluene solutions of S-4 at various concentrations at room temperature.

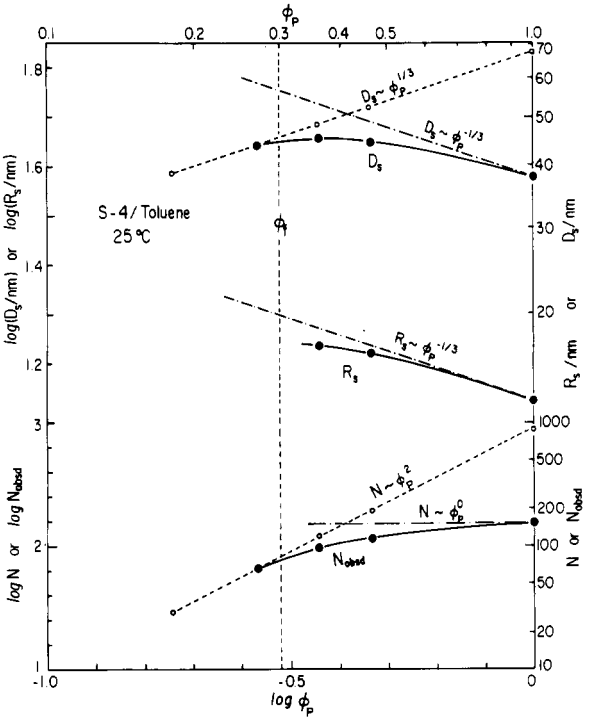


**Figure 5.** Concentration dependence of the size of the spherical microdomains $R_s$, the Bragg spacing $D_s$, and the average number of block chains per spherical microdomain for a toluene solution of S-4 at 25 °C. $\phi_P$ is polymer volume fraction and $\phi_f$ is the critical $\phi_P$, above which the nonequilibrium effect becomes increasingly important.

although the value $\phi_f$ for the spherical domain is *much smaller* than that for the lamellar domains and results from the nonequilibrium effect on microdomain formation as will be discussed in detail in section IV. The nonequilibrium effect accounts for the large discrepancies between the measured and calculated $D_s$ and $R_s$ in the bulk specimens as seen in Figure 2.

The SAXS profiles were also investigated as a function of temperature at a given concentration (e.g., 50.4 wt %). The change of the Bragg spacing $D_s$ with temperature is

Table II
Bragg Spacing $D_s$ and Radius of the Spherical Domains $R_s$ As Estimated by SAXS and the Volume Fractions of the Spherical Domains $\phi_d$ in the Solution As Estimated from Eq III-6 and III-7 for Toluene Solutions of S-4

| wt % polymer concn | domain size estd by SAXS | | vol fraction of spherical domain $\phi_d$ | | | |
|---|---|---|---|---|---|---|
| | $D_s$,[a] nm | $R_s$,[b] nm | $\phi_{d,calcd}$[c] | $\phi_{d,sc}$[d,e] | $\phi_{d,bcc}$[d,e] | $\phi_{d,fcc}$[d,e] |
| 40.2 | 45.6 | 17.9 | 0.167 | 0.253 | 0.179 | 0.195 |
| 50.4 | 44.5 | 17.7 | 0.167 | 0.263 | 0.186 | 0.203 |
| 100 | 38.0 | 13.3 | 0.167 | 0.180 | 0.127 | 0.138 |

[a] Estimated from eq III-1. [b] Estimated from eq III-2. [c] Estimated from eq III-7. [d] Estimated from eq III-6. [e] $\phi_{d,sc}$, $\phi_{d,bcc}$, and $\phi_{d,fcc}$ stand for volume fraction of the spherical domains in the solution for sc, bcc, and fcc lattices, respectively.

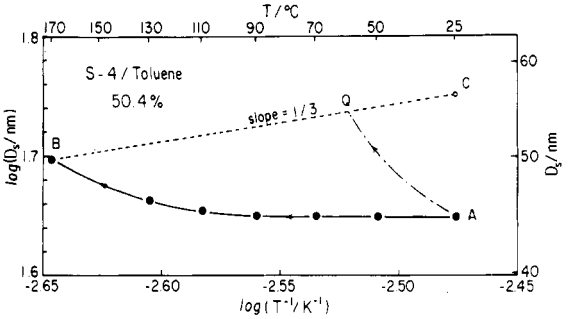


**Figure 6.** Variation of the Bragg spacing $D_s$ for the 50.4 wt % toluene solution of S-4 during heating and cooling cycles.

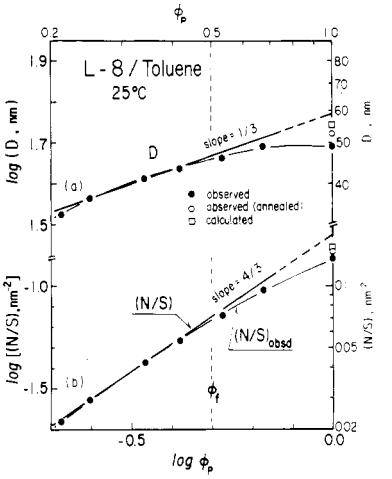


**Figure 7.** Concentration dependence of (a) the lamellar identity period $D$ and of (b) the average number of block chains per unit interfacial area for a toluene solution of L-8 at 25 °C. $\phi_P$ and $\phi_f$ have the same meaning as in Figure 5. The calculated value (open square) was obtained from Meier's and Helfand and Wasserman's theories.

shown in Figure 6 for the 50.4 wt % toluene solution. The $D_s$ value tends to increase with increasing $T$, which is opposite to what we expect from arguments based on thermodynamic equilibrium, as will be discussed in detail in section IV. Our conclusion is that the increase of $D_s$ with $T$ is a consequence of the system at room temperature being far from equilibrium, having $D_s$ much less than the equilibrium values at higher temperatures. The increase of the temperature causes the system to reach the equilibrium value at each temperature, which should result in the observed increase of $D_s$'s.

**(b) Packing of Spherical Microdomains.** We now consider spatial packing of the spherical microdomains in the concentrated solutions. It is worth noting that the spatial packing of the spherical domains in bulk has been reported by a number of investigators.[6,11,29-32,43] The controversy existing in the reported results has recently been pointed out and discussed by Bates, Cohen, and Berney.[32] Here, we adopt the same principle as employed in these earlier works to study the packing in the solution. It is obvious from the relative peak positions that the packing is likely to be either simple cubic (sc) or body-centered cubic (bcc). The measured Bragg spacing $D_s$ is related to the cell edge $a_c$ of the cubic lattice and the nearest-neighbor distance of the spheres $D_0$

$$D_s = a_c = D_0 \quad \text{for sc} \qquad \text{(III-3)}$$

$$D_s = a_c/2^{1/2} = (2/3)^{1/2}D_0 \quad \text{for bcc} \qquad \text{(III-4)}$$

$$D_s = a_c/3^{1/2} = (2/3)^{1/2}D_0 \quad \text{for fcc} \qquad \text{(III-5)}$$

where fcc stands for face-centered cubic. The volume fraction of the spherical microdomains $\phi_d$ may be calculated for $a_c$ and $R_s$

$$\phi_d = \frac{4\pi}{3}k\left(\frac{R_s}{a_c}\right)^3 \qquad \text{(III-6)}$$

where $k$ is a packing constant; $k = 1$, 2, and 4 for sc, bcc, and fcc. The $\phi_d$ values estimated for sc, bcc, and fcc are listed in Table II. The volume fraction $\phi_d$ may also be estimated from a given partition of the solvent to the domains $\alpha_d$ on the basis of no volume change of mixing and of no mixing[23] of the unlike segments in each microphase.

$$\phi_{d,calcd} = \phi_P\phi_{PS} + \alpha_d(1 - \phi_P) \qquad \text{(III-7)}$$

where $\phi_P$ and $\phi_{PS}$ are the volume fraction of the block polymer in solution and the volume fraction of polystyrene in the block polymer, respectively. Table II indicates the results of $\phi_{d,calcd}$. The mass densities of polystyrene, polyisoprene, and toluene are 1.052, 0.925, and 0.87 g/cm$^3$, respectively. The value of $\alpha_d$ equals 0.164, i.e., the volume fraction of the polyisoprene in the block polymer for the neutral solvents.

It is shown that the $\phi_{d,calcd}$ values are approximately equal to $\phi_{d,bcc}$ for 40.2 and 50.4 wt % solution but to $\phi_{d,sc}$ for bulk polymer. Thus the volume consideration suggests that a probable structure is bcc for the concentrated solutions and sc for bulk. The volumetric analysis on our previous data for the spherical domains in bulk[11] also suggests that sc may be a probable structure for bulk. The change of the packing from bcc to sc is not well understood at present. We believe, however, the rigorous assignment of the packing deserves further attention, especially some analysis of the relative peak heights of the interparticle interference maxima.

**2. Lamellar Microdomains.** In the previous papers[7,13] we studied the development of lamellar microdomains with increasing polymer concentration $\phi_P$ with neutral solvents and presented results that showed the lamellar spacing $D$ tends to *increase* with $\phi_P$ due to *increasing segregation power* between A and B in AB block polymers in the presence of the solvents. The results are shown in Figure 7a for a toluene solution of L-8 at 25 °C. It should be noted that the $D$ value in bulk (49.2 nm) is slightly but significantly smaller than the value (58.9 nm) extrapolated to

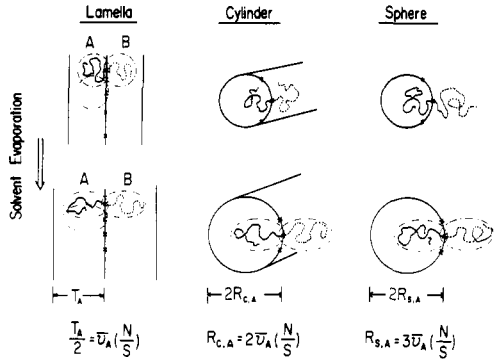


**Figure 8.** Schematic diagram showing growth of three fundamental microdomains involved by increasing polymer concentration.

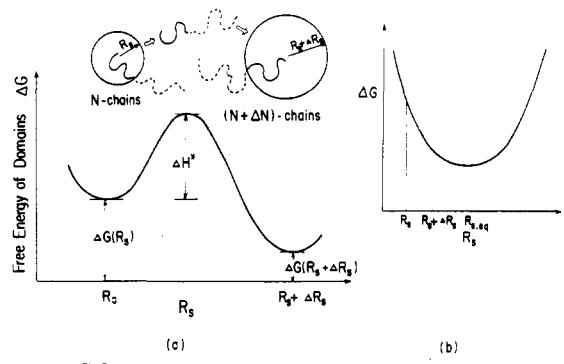


**Figure 9.** Schematic diagrams showing (a) potential barrier $\Delta H^*$ for the growth of spherical microdomains from $R_s$ to $R_s + \Delta R_s$ and (b) free energy $\Delta G$ of the spherical microdomain as a function of $R_s$.

zero solvent concentration. Subsequent annealing of the as-cast films at 120 °C for 8 h increases the $D$ value to a value (52.7 nm) close to the extrapolated value. We propose in section IV that these effects are due to a nonequilibrium effect of microdomain formation significant at concentrations greater than $\phi_f$.

## IV. Discussion

**1. Model for Growth of Microdomains.** It might be puzzling and disturbing at first glance to accept the experimental evidence that the lamellar spacing increases with increasing polymer concentration $\phi_P$ in view of (i) the increasing deswelling effect with $\phi_P$, the effect of which may decrease $D$ with $\phi_P$, and (ii) the decreasing dimensions of the polymer coils with $\phi_P$ due to the increasing screening effect of excluded volume effects.[33,34] We have demonstrated, however, in our previous papers[7,13] that this experimental evidence is a natural, but not surprising, consequence of the segregation effect outweighing the two effects described above. This point will be described below in more detail because the segregation effect is proposed here to be the one commonly involved in the concentration dependence of the spherical domains.

As the concentration of solution increases or its temperature decreases, the effective segregation power between A and B polymers in the presence of solvent increases, which tends to drive the domains to grow in equilibrium situation, so as to reduce the surface-to-volume ratio. Figure 8 schematically shows this effect on the domain growth, as encountered by solvent evaporation. As the segregation power increases, the A and B chains tend to be stretched more perpendicular to the interfaces, resulting in an increase of their end-to-end distances and hence in an increasing lamellar thickness $T_A$, radius of cylindrical ($R_{c,A}$) or spherical domains ($R_{s,A}$), and their interdomain distances. The resulting loss of the conformational entropy and loss of the entropy of placing the chemical junction points in the interfacial region are outweighed by the decrease of the interfacial energy. Hence equilibrium should favor the domain growth. In fact, the equilibrium theories developed by Meier[8,9] and Helfand[3] predict that the lamellar thickness increases with increasing $\chi$, the Flory–Huggins interaction parameter[33] between the block chains. It can be shown from Noolandi and Hong's theory[4] that the thickness increases with increasing polymer concentration $\phi_P$.[13] There is a small decrease of polymer coil dimensions with increasing $\phi_P$ even in the concentration range we studied here due to the increasing degree of screening of the excluded volume effect, which tends to decrease the domain size even in the equilibrium regime. However, our experimental results show this effect is outweighed by the segregation effect.

This increase of the domain size $T_A$, $R_{c,A}$, or $R_{s,A}$ must be accompanied by a decrease of the average neighbor distance $a$ between the chemical junction points along the interface or by an increase in the number of chains per unit interfacial area, $N/S$, as may be obvious from the volume consideration

$$\begin{aligned} T_A/2 &= \bar{v}_A(N/S) \\ R_{c,A} &= 2\bar{v}_A(N/S) \\ R_{s,A} &= 3\bar{v}_A(N/S) \end{aligned} \qquad \text{(IV-1)}$$

where $\bar{v}_A$ is the volume occupied by a single block chain A in the presence of the solvents. It should be noted that if $N/S$ or $a$, which is defined as

$$a \equiv (S/N)^{1/2}$$

is kept constant during solvent evaporation, the increase of the polymer concentration $\phi_P$ results in *decreases* of $T_A$, $R_{c,A}$, and $R_{s,A}$, because $\bar{v}_A$ decreases with $\phi_P$.

The increase of $N/S$ or decrease of $a$ involves displacement of the chemical junction points along the flat and curved interfaces for lamellar and cylindrical microdomains, respectively. The relaxation time for the displacement depends on $\phi_P$, generally increasing with increasing $\phi_P$. If the relaxation time is short compared with the experimental time scale, then the system can achieve equilibrium and the domain size is *thermodynamically controlled*, increasing with increasing $\phi_P$. However, if the relaxation time is much larger than the time scale of the experiment, the value of $N/S$ or $a$ is essentially *frozen in* to a fixed value. Thus the system is in *nonequilibrium* in terms of $N/S$ or $a$ but is in equilibrium in terms of the chain conformations: the system is in *microequilibrium* or *local equilibrium* having minimum free energy for a given value of $N/S$ or $a$. Further increase of $\phi_P$ with a fixed value of $N/S$ or $a$ results in shrinkage of $T_A$ and $R_{c,A}$ simply by *deswelling*, i.e., by decreasing $\bar{v}_A$ in eq IV-1. In this regime of $\phi \geq \phi_f$, $\phi_f$ being the concentration where $N/S$ or $a$ is *virtually frozen in*, the size of the domain is *kinetically controlled*.

The spherical domains can change their size $R_{s,A}$ or $N/S$ or $a$ only by a process involving transport of A chains through the matrix of B chains. This process involves *thermodynamic interactions* between A and B as well as the *frictional interactions* as encountered in the growth of the lamellar and cylindrical domains. Figure 9 schematically illustrates the potential barrier for the growth of the spherical domains. Suppose that there is a thermodynamic driving force for the domain to grow from $R_s$ to $R_s + \Delta R_s$: the free energy of the domains $\Delta G$ satisfying $\Delta G(R_s + \Delta R_s) < \Delta G(R_s)$ as shown in Figure 9b. The

growth of the domain involves the transport of the block chain as described above and as depicted in Figure 9a.

The potential barrier for the transport process $\Delta H^*$ depends both on thermodynamic ($\Delta H_{therm}$) and frictional interaction energies ($\Delta H_{frict}$).

$$\Delta H^* = \Delta H_{therm} + \Delta H_{frict} \quad \text{(IV-2)}$$

$\Delta H_{therm}$ depends on the heat of mixing of A and B in the presence of solvent. For the neutral solvent, equally good for A and B,

$$\Delta H_{therm}/k_BT \sim \chi_{AB}\phi_P \quad \text{(IV-3)}$$

where

$$\chi_{AB} = (\delta_A - \delta_B)^2/\rho_0 k_B T \quad \text{(IV-4)}$$

$\chi_{AB}$ is the Flory–Huggins interaction parameter between A and B in bulk, $\delta_K$ is the solubility parameter of K (K = A or B), $k_B$ is the Boltzmann constant, and $\rho_0$ is the number density of the monomer unit. Thus the *thermodynamic potential barrier* is proportional to polymer volume fraction $\phi_P$ but is essentially *independent of molecular weight*. On the other hand, the *frictional potential barrier* should strongly depend on molecular weight. Thus the potential barrier for the growth of the spherical domains is generally much larger than that for the growth of cylindrical and lamellar microdomains. This accounts for the peculiar phenomena observed for the spherical microdomains as observed in Figure 2. In other words, the relaxation time $\tau_s$ for the spherical domains

$$\tau_s = \tau_{0,s} \exp(-\Delta H^*/k_BT) \quad \text{(IV-5)}$$

should be much longer than that for the cylindrical and lamellar microdomains, which primarily depends only on $-\Delta H_{frict}$.

$$\tau_M = \tau_{0,M} \exp(-\Delta H_{frict}/k_BT) \quad \text{(IV-6)}$$

where M is for either cylindrical or lamellar microdomain. It is therefore expected that the *crossover concentration* $\phi_f$ should be much lower for the spherical domains than for the cylindrical and lamellar microdomains. The relaxation time and $\phi_f$ for the spherical domains may have a molecular weight dependence different from those for the lamellar and cylindrical domains.

**2. Possible Analysis of Nonequilibrium Effect on Microdomains.** On the basis of the arguments described in the preceding section, we now present a possible approach for the nonequilibrium effect on the microdomains.

**(a) Nonequilibrium Effects in Lamellar Microdomains.** In the previous papers[7,13] we found that in the segregation limit the thermodynamically controlled domain size of lamellar microdomains in neutral solvents varies with $\phi_P$ and absolute temperature $T$ according to

$$D \equiv T_A + T_B \sim (\phi_P/T)^{1/3} \quad \text{(IV-7)}$$

where $D$ is the lamellar identity period[24] and $T_A$ and $T_B$ are the thicknesses of the A and B lamellae, respectively. If eq IV-7 is valid for all concentrations up to bulk, one predicts the $D$ value in bulk to be 58.9 nm, which is in good agreement with the equilibrium $D$ values of 57.6 and 55.4 nm predicted from the Meier[9] and Helfand[3] theories, respectively.

The measured $D$ value (49.2 nm) is significantly smaller than the value (58.9 nm) extrapolated to $\phi_P = 1$, which we propose is due to the *nonequilibrium effect* as discussed in the preceding section. That is, with increasing $\phi_P$, the two-dimensional displacement of the chemical junction points along the interfaces is dramatically slowed down. Consequently at concentrations higher than the critical concentration $\phi_f$, the value of $a$ or $N/S$ is virtually frozen in on the time scale of the experiment. The systems attain *microequilibrium* or *local equilibrium* with a given frozen-in value of $a$ or $N/S$, resulting in decreasing or levelling off of $D$ with increasing $\phi_P$ simply due to deswelling of the solvent, i.e., a decrease of $\bar{v}_A$.

Further annealing of the as-cast film at 120 °C for 8 h enhances the system reaching equilibrium at that temperature, e.g., 120 °C. The specimen was then cooled down to room temperature. During cooling the specimen tends to attain a new equilibrium. The equilibrium $D$ value should increase with a lowering of the temperature from 120 to 25 °C, for example, according to eq IV-7. It should increase from 51.0 to 55.4 nm according to HW theory.[3] However, the response of the $D$ value in a real system depends on the rate of cooling and is essentially quenched at the glass transition temperature of polystyrene. The overall thermal history involved in this annealing process gives rise to the increased $D$ value as shown in Figure 7a (open circle, 52.7 nm). The $D$ value increases with the annealing since the $D$ value for the as-cast specimen is less than the value expected for equilibrium at 25 °C and is even less than the equilibrium value at higher temperatures. At $\phi < \phi_f$, $D$ values vary reversibly with $T$ according to eq IV-7. Figure 11 shows an example of this tendency, although much better reversibility is obtained at lower concentrations or at lower heating and cooling rates.

It is useful to argue the *nonequilibrium effect* in terms of $N/S$, the average number of chains emanating per unit interfacial area. If eq IV-7 is valid up to $\phi_P = 1$, one predicts $N/S$ increases with $\phi_P$ according to

$$N/S \sim \phi_P^{4/3} \quad \text{(IV-8)}$$

from eq IV-1 and IV-7. One can estimate the real response of $N/S$ [$(N/S)_{obsd}$, shown by filled circles] from the concentration dependence of $D$ based upon the equation of Sadron and Gallot[17]

$$(N/S)_{osbd} = \left(\frac{DCN_A}{2M}\right)^2 \{C[w_{PS}/d_{PS} + (1 - w_{PS})/d_{PI}] + (1 - C)/d_S\}^{-2} \quad \text{(IV-9)}$$

where $w_K$ is the weight fraction of K-block chain (K = PS or PI) in block polymer, $d_K$ and $d_S$ are the mass densities of K polymer and solvent, respectively, $C$ is the weight fraction of polymer in solution, $M$ is the total molecular weight of the block polymer, and $N_A$ is Avogadro's number. Figure 7b shows a comparison of $N/S$ predicted from eq IV-8 and $(N/S)_{obsd}$ estimated from eq IV-9. It is obvious that $(N/S)_{obsd}$ increases with $\phi_P$ according to eq IV-8 at low concentrations $\phi_P < \phi_f$ but that it levels off and becomes smaller than $N/S$ at high concentrations $\phi_P > \phi_f$ owing to the *nonequilibrium effect* as already discussed. The crossover concentration $\phi_f$ is about 0.5 for this particular solution and is a function of molecular weight for a given time scale of the experiment and of time scale of the experiment for a particular solvent–polymer combination.

The $(N/S)_{obsd}$ value for $\phi_P = 1$ is much less than the extrapolated value and increases with the annealing process as described above.

**(b) Nonequilibrium Effect in the Spherical Microdomains: Concentration Dependence.** The increase of the segregation power with $\phi_P$ should also increase the Bragg spacing $D_s$ and the radius $R_s$ of the spherical domain. It may be reasonable to assume that in the equilibrium regime, $D_s$ and $R_s$ also increase according to eq IV-7

$$D_s, R_s \sim (\phi_P/T)^{1/3} \quad \text{for } \phi_P < \phi_f \quad \text{(IV-10)}$$

The spherical microdomain systems are markedly different from the lamellar microdomain in that the concentration $\phi_f$ for the spherical systems should be much lower than that for the lamellar system due to the extra potential energy $\Delta H_{therm}$ for the growth of the domain as discussed in section IV-1 (eq IV-2 and IV-3).

For the spherical domains

$$a_c^3 = kN(\bar{v}_A + \bar{v}_B) \qquad \text{(IV-11)}$$

where $k$ is again the packing constant equal to 1, 2, and 4 for sc, bcc, and fcc, respectively; $a_c$ is the cell edge of the lattice that is related to the Bragg spacing $D_s$ (eq III-3–III-5). Since $\bar{v}_A + \bar{v}_B \sim \phi_P^{-1}$, the average number of chains per spherical domain $N$ is given by

$$N \sim \phi_P^2 \qquad \text{(IV-12)}$$

if the packing constant $k$ is independent of $\phi_P$. Thus if $D_s$ and $R_s$ increase with $\phi_P$ according to eq IV-10 in the equilibrium regime ($\phi_P < \phi_f$), then $N$ should increase according to eq IV-12. The number $N$ can also be estimated from the measured $D_s$ according to[17]

$$N_{obsd} = \frac{CN_A a_c^3}{kM}\{[w_{PS}/d_{PS} + (1 - w_{PS})/d_K]C + (1 - C)/d_S\}^{-1} \qquad \text{(IV-13)}$$

$d_K$ is the mass density of polymer K, which is polybutadiene for the SB polymer or polyisoprene for the S-4 polymer.

It is clearly shown in Figure 5 that the experimental results on $D_s$, $R_s$, and $N_{obsd}$ (solid circles) do not obey eq IV-10 and IV-12 (expected for the thermodynamically controlled microdomains) at polymer concentrations higher than 30.5 wt % ($\phi_P$ = 0.270) where the clear discrete scattering maxima are observed (see Figure 4). If we assume that the concentration of $\phi_P$ = 0.3 is the upper limit of the concentrations where the microdomains are thermodynamically controlled (i.e., $\phi_f \simeq 0.3$), then the observed changes of $D_s$, $R_s$, and $N_{obsd}$ with $\phi_P$ are due to the *nonequilibrium effect* arising from the increased potential barrier for the growth of the domian. That is, the increase of $N_{obsd}$ with $\phi_P$ is slowed down and becomes much less than the predicted value of $N$ as shown in Figure 5, which, in turn, results in the measured $D_s$ being much less than the predicted $D_s$ as shown in Figure 5. The assumption that the microdomains at $\phi_P$ = 0.270 (30.5 wt % polymer solution) are close to equilibrium may be fairly good in view of the experimental results showing a reversible change of the SAXS profiles with temperature as shown in Figure 3.

The dash–dot lines in Figure 5 indicate the hypothetical variations of $D_s$, $R_s$, and $N$ with $\phi_P$ involved by swelling of the microdomains in bulk with a fixed value of $N$. It is obvious from eq IV-11 and from the following equations

$$\frac{4\pi}{3}R_{s,K}^3 = N\bar{v}_K \qquad \text{(K = A or B)} \qquad \text{(IV-14)}$$

$$\bar{v}_K = \frac{M_K}{d_K\phi_P N_A} \qquad \text{(K = A or B)} \qquad \text{(IV-15)}$$

that $R_s$ and $D_s$ scale as $\phi_P^{-1/3}$ under this condition. In eq IV-14 and IV-15, $R_{s,K}$ is the radius of the microdomain composed of K-block chains and the neutral solvent. If $N$ increases with $\phi_P^2$ at low concentrations as shown by the broken line and is frozen in around $\phi_P \simeq 0.4$ and kept constant with further increase of $\phi_P$ as shown by the dash–dot line, then the value of $D_s$ would first increase with $\phi_P$ according to $\phi_P^{1/3}$ along the broken line and subsequently decrease with further increase of $\phi_P$ ($\gtrsim$0.4) according to $\phi_P^{-1/3}$ along the dash–dot line. In a real system, $N_{obsd}$ asymptotically approaches a constant value, thus resulting in gradual changes of $D_s$ and $R_s$ with $\phi_P$ as shown in the experimental results (filled circles).

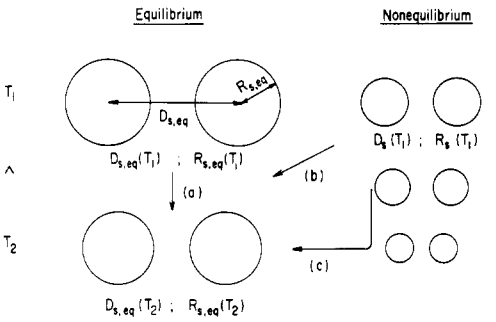


**Figure 10.** Schematic diagrams showing variations of the radius of the spherical microdomain and of the interdomain distance upon elevating temperature from $T_1$ to $T_2$ under equilibrium (process a) and nonequilibrium conditions (processes b and c).

If $D_s$ increases with $\phi_P$ on the broken line shown in Figure 5, $D_s$ approaches about 70 nm in bulk, which is much larger than about 40 nm for the observed value of $D_s$ at $\phi_P$ = 1. The estimated equilibrium value of 70 nm is very close to 87 nm (interparticle distance) calculated from HW theory.[3,11] It should be noted that the sample S-4 corresponds to the sample SI-4 in ref 11. The changes of $D_s$ and $R_s$ accompanied by such correction as described above are also indicated in Figure 2 by the data points marked by solid diamond-shaped arrows. Our previous analyses[11] indicated that the ratio of the observed values $D_s$ and $R_s$ was in good agreement with HW theory, from which we proposed that the spherical microdomains we observed are nonequilibrium in terms of $N$ only. By assuming a constant value of $D_s/R_s$, we can also estimate the corrected value of $R_s$ at $\phi_P$ = 1, the value being 23.3 nm and included in Figure 2. The value $R_s$ calculated from HW theory is 26.7 nm.

**(c) Nonequilibrium Effect in the Spherical Microdomains: Temperature Dependence.** We now give an interpretation on the temperature dependence of the 50.4 wt % toluene solution of S-4 shown in Figure 6. In Figure 10 we show a schematic diagram to account for the temperature dependence. In equilibrium, the values $D_s$ and $R_s$ should decrease from $D_{s,eq}(T_1)$ and $R_{s,eq}(T_1)$ to $D_{s,eq}(T_2)$ and $R_{s,eq}(T_2)$ with increasing temperature from $T_1$ to $T_2$ as shown in process a of Figure 10. In a real system the microdomains have the values $D_s(T_1)$ and $R_s(T_1)$, much less than the equilibrium values as already discussed. The increase of the values with increasing temperature is best interpreted as a consequence of the system approaching the equilibrium as shown in process b in Figure 10. The value of $D_s$ increases because the value at low temperature $T_1$ is even less than the equilibrium values at higher temperature $T_2$'s. [i.e., $D_s(T_1) < D_{s,eq}(T_2)$ and $R_s(T_1) < R_{s,eq}(T_2)$] as shown in Figure 10. At higher temperatures the relaxation time to achieve equilibrium ($\tau_s$ in eq IV-5) becomes shorter because the potentials $\Delta H_{therm}$ and $\Delta H_{frict}$ drop. Hence the value of $D_s$ tends to increase at a high rate as shown in Figure 6. The change of $D_s$ with $T$ (as shown from the points A to B in Figure 6) should really depend on a heating rate relative to the rate of equilibration ($1/\tau_s$). It might change from the points A to Q and Q to B, depending upon the thermal history. The heating rate employed in this experiment was approximately 5 °C/h.

The broken line indicates the hypothetical variation of $D_s$ upon cooling that may occur if the spherical domains

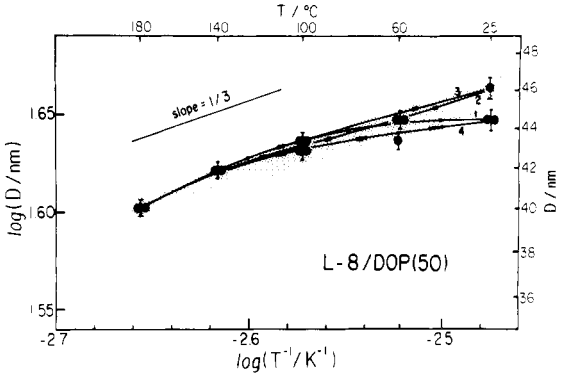


**Figure 11.** Thermal hysteresis on the lamellar identity period $D$ for a 50 wt % DOP solution of L-8.

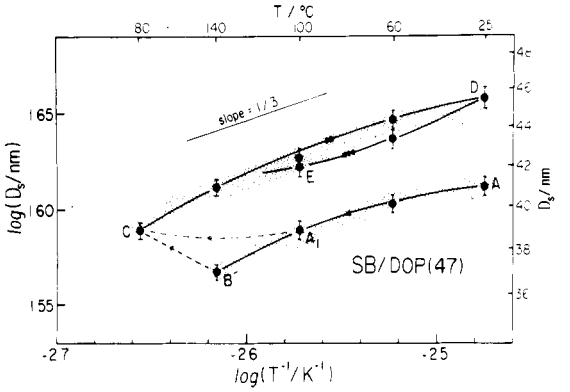


**Figure 12.** Thermal hysteresis on the Bragg spacing $D_s$ for a 47 wt % DOP solution of SB.

grow in equilibrium from the value at 170 °C according to eq IV-10. The extrapolated value at 25 °C (about 56 nm) is close to the equilibrium value predicted from the broken line in Figure 5 (about 52 nm).

**3. Further Remarks on Nonequilibrium Effects.** Here we present further the nonequilibrium effects on the spherical and lamellar microdomains as observed in the temperature hysteresis of the Bragg spacings of the lamellar microdomains ($D$) and spherical microdomains ($D_s$).

Figures 11 and 12 show, respectively, the temperature hysteresis of $D$ for a 50 wt % DOP solution of L-8 and of $D_s$ for a 47 wt % DOP solution of SB. The DOP solutions of L-8 showed the SAXS profiles typical of the lamellar microdomains, while the DOP solution of SB showed those typical of the spherical microdomains. It should be noted that the nonequilibrium effect with DOP is not identical with that with toluene, since when DOP is used as a solvent we must consider the microdomain formation and its nonequilibrium effect in the mixed solvent of DOP and methylene chloride for a given evaporation rate of methylene chloride. However, the two DOP systems would be useful to compare the nonequilibrium effects encountered in the lamellar and spherical domain systems, because they have about the same concentrations and total molecular weights.

For given heating (50 °C/h) and cooling rates (50 °C/h), the response of the lamellar microdomains (Figure 11) is much more reversible than that of the spherical microdomains (Figure 12), indicating that the lamellar microdomains are much more close to equilibrium than the spherical microdomains at a given concentration (47–50 wt % polymer). The lamellar domains show an almost reversible response according to eq IV-10. The reversibility is nearly perfect at temperatures higher than 100 °C, where the equilibration rate ($1/\tau_{lam}$, $\tau_{lam}$ being the relaxation time for the equilibration of the lamellar microdomians) should be faster than the rate of the thermal stimulus.

The value of $D_s$ of the spherical domain decreases with increasing $T$ from point A to B and increases from point B to C with further increase of $T$. Upon cooling from 180 to 25 °C, $D_s$ increases from point C to D. The value decreases from point D to E in the second heating cycle, close to the locus of D to C. The change of the value of $D_s$ in the thermal processes from C to D and D to E is, more or less, reversible and obeys approximately eq IV-10.

It is interesting to note that the value of $D_s$ changes approximately according to eq IV-10 in the thermal process of A to B in the first heating cycle for this particular specimen rather than changingfrom point A to $A_1$ and $A_1$ to C, for example, as we found in Figure 6. This peculiar response, quite different from that shown in Figure 6 and also from that shown schematically in process b in Figure 10, may be best understood as a consequence of the system achieving *local equilibrium* (or *microequilibrium*) in the process A to B. At point B, memory of the initial microdomains is essentially lost and the system tends to achieve equilibrium with a further increase of $T$, resulting in the upturn behavior from B to C. This peculiar response may be schematically explained by process c in Figure 10. The difference in the response shown in Figure 6 (A to B or hypothetical A to Q to B) and that in Figure 12 (A to B to C or hypothetical A to $A_1$ to C) is believed to arise from the difference of the heating rate relative to the equilibration rate ($1/\tau_s$). It should be noted that the heating rate for the DOP solution (Figure 12) is much faster (by a factor of 10) than that for the toluene solution (Figure 6).

It may be noted that the temperature dependence of $D_s$ is very small and almost negligible within the accuracy of the measurements in the low-temperature range from 25 to about 60 °C. In this temperature range the transport of molecules from one domain to another is considered to occur with a time scale much larger than the time scale of the experiment. However, at higher temperatures, the transport rate becomes increasingly large so that the system may attain equilibrium, resulting in the response of $D_s$ with $T$ as predicted by eq IV-1.[10]

**4. Lattice Disordering and Domain-Boundary Thickness. (a) Lattice Disordering.** In our previous paper[18] we discussed the line profile of the scattering maxima arising from the interparticle interference of the spherical microdomains and showed that the integral breadths of the maxima are reciprocally proportional to the coefficient $f$ (i.e., the "*spring constant*") of the *quasi-elastic restoring force* of the lattice (composed of the spherical microdomains) with respect to the displacement from the equilibrium state. We further pointed out that this quasi-elastic restoring force can be calculated from the change of the free energy of the microdomain systems accompanied by distortion from the equilbium state. $N_{AB}(T)$ in ref 18 may also be read as the number of *elastically active chains* at temperature $T$, whose meaning will be briefly discussed below.

We further advanced the studies of the line profile in bulk polymers to the spherical microdomains existing in a selective solvent and showed that the quasi-elastic restoring force or elastic modulus of the solutions originates primarily from the *entropy elasticity of the confined chains* and hence is proportional to polymer concentration $\phi_p$ of the solution.[19] The variation of the line profile with concentration shown in Figure 3 also may be explained based on the arguments described in ref 18 and 19. The elastically active chains are those whose A- and B-block

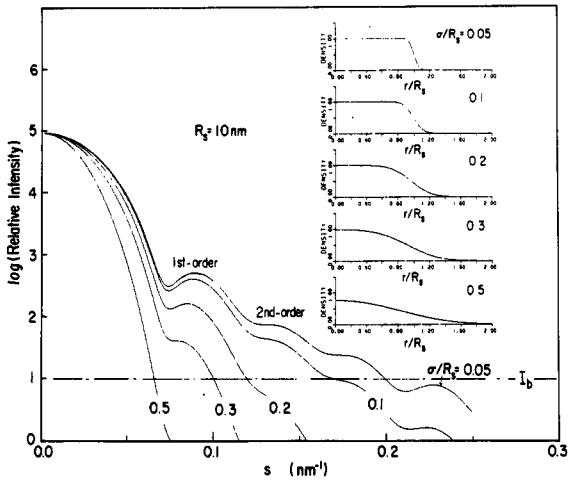


**Figure 13.** Effect of the diffuseness of the domain-boundary region on the SAXS profiles from the isolated spherical domains: $\sigma/R_s = 0.05$, $\sigma/R_s = 0.1$, $\sigma/R_s = 0.2$, $\sigma/R_s = 0.3$, and $\sigma/R_s = 0.5$. The corresponding relative electron density profiles $\Delta\tilde{\rho}(r)$ are shown in the upper right-hand corner of the figure.

chains are properly segregated into A domains and B matrix, respectively. When $D_s$ and $R_s$ are perturbed from their equilibrium values, these chains contribute to the increase of free energy of the system, thus contributing to the elastic restoring force. However, the energy stored in the system or individual chains may be partially dissipated if a number of A-block chains are pulled out from the A domains into the B matrix, resulting in a decreased elastic restoring force. The number of chains that are pulled out from the domains before and after perturbing the system from equilibrium, defined as *elastically ineffective chains*, increases with increasing temperature and causes the increasing line broadening with temperature. It may be noted that the enhanced mobility of the chemical junction points of the block polymers in the interfacial region with temperature may give an effect similar to that discussed above and also cause a reduction of elastic restoring force and the line broadening, although this point is not suggested in the previous paper.[19]

**(b) Effect of Diffuse Domain Boundary on SAXS Profiles.** The technique to estimate quantitatively the narrow interfacial thickness of the domain-boundary region was explored and discussed by many investigators.[6,10,11,16,18,21,25,35-42,44] Here, we focus our interests only on the effect of increasing interfacial thickness on the whole scattering profiles in connection with the arguments put forward in section III-1-a. The sigmoidal electron density variation across the diffuse boundary $\rho_{obsd}(\mathbf{r})$ may be given by a convolution product of the electron density variation of the system having a sharp boundary $\rho_i(\mathbf{r})$ and the Gaussian smoothing function $h(\mathbf{r})$ with a variance $\sigma^2$ after Ruland.[25]

Figure 13 shows computer simulation of the effect of the diffuse boundary on the scattering from isolated spheres with an average radius of sphere $R_s = 10$ nm, standard deviation $\sigma_R = 0.1R_s$ for the fluctuation of the sphere size, and diffuse boundaries as characterized by $\sigma/R_s = 0.05$, 0.1, 0.2, 0.3, and 0.5. The profiles of the excess electron density of the sphere $\Delta\tilde{\rho}(r) = \Delta\rho_s(r)/\Delta\rho_0$ with respect to the matrix is shown as a function of $r$ in the upper right-hand corner of the figure ($\Delta\rho_0 \equiv \rho_s - \rho_m$, $\rho_s$ and $\rho_m$ being the electron densities of the sphere and matrix, respectively, in the case of the sharp boundary). The results clearly indicate that the larger the $s$, the greater is the effect of the diffuse boundary. If the background scattering arising from thermal diffuse scattering has an intensity level $I_b$ as drawn by the dash-dot line in the figure, higher order peaks up to the third order may be resolved but the fourth-order peak may be buried in the background level in the case of $\sigma/R_s = 0.1$. In the case of $\sigma/R_s = 0.2$, only the first-order peak may be resolved, and in the case of $\sigma/R_s = 0.5$, the first-order peak also may be smeared in the background level. This effect of diffuse boundary therefore may account for the experimental evidence that, with decreasing polymer concentration, the higher order scattering maxima disappear without significantly affecting the breadth of the lower order scattering maxima.

**Acknowledgment.** We express our sincere thanks to Mr. H. Watanabe and Professor T. Kotaka, Department of Polymer Science, Faculty of Science, Osaka University, Japan, for supplying the SB block polymers. Part of this work is supported by a grant from the U.S.-Japan Cooperative Research Program of the NSF and the JSPS and by a Grant-in-Aid for Special Project Research from the Ministry of Education, Japan (57119003).

**Registry No.** Styrene/isoprene copolymer, 25038-32-8; styrene/butadiene copolymer, 9003-55-8.

## References and Notes

(1) Krause, S. *J. Polym. Sci., Polym. Phys. Ed.* **1969**, *7*, 249; *Macromolecules* **1970**, *3*, 84.
(2) Meier, D. J. *Org. Coat. Plast. Chem.* **1977**, *37* (1), 246.
(3) Helfand, E.; Wasserman, Z. R. *Macromolecules* **1976**, *9*, 879; **1978**, *11*, 960; **1980**, *13*, 994.
(4) Noolandi, J.; Hong, K.-M. *Ferroelectrics* **1980**, *30*, 117.
(5) Leibler, L. *Macromolecules* **1980**, *13*, 1602.
(6) Roe, R.-J.; Fishkis, M.; Chang, C. J. *Macromolecules* **1981**, *14*, 1091.
(7) Hashimoto, T.; Shibayama, M.; Kawai, H. *Macromolecules* **1983**, *16*, 1093 (part 4 of this series).
(8) Meier, D. J. *J. Polym. Sci., Part C* **1969**, *26*, 81.
(9) Meier, D. J. *Prepr. Polym. Colloq., Soc. Polym. Sci., Jpn., Kyoto* **1977**, 83.
(10) Hashimoto, T.; Shibayama, M.; Kawai, H. *Macromolecules* **1980**, *13*, 1237.
(11) Hashimoto, T.; Fujimura, M.; Kawai, H. *Macromolecules* **1980**, *13*, 1660.
(12) Shibayama, M.; Hashimoto, T.; Kawai, H. *Macromolecules* **1983**, *16*, 16 (part 1 of this series).
(13) Shibayama, M.; Hashimoto, T.; Hasegawa, H.; Kawai, H. *Macromolecules* **1983**, *16*, 1427 (part 3 of this series).
(14) Hashimoto, T.; Suehiro, S.; Shibayama, M.; Saijo, K.; Kawai, H. *Polym. J.* **1981**, *13*, 501.
(15) Fujimura, M.; Hashimoto, T.; Kawai, H. *Mem. Fac. Eng., Kyoto Univ.* **1981**, *43* (2), 224.
(16) Todo, A.; Hashimoto, T.; Kawai, H. *J. Appl. Crystallogr.* **1978**, *11*, 558.
(17) Sadron, C.; Gallot, B. *Makromol. Chem.* **1973**, *164*, 301.
(18) Fujimura, M.; Hashimoto, H.; Kurahashi, K.; Hashimoto, T.; Kawai, H. *Macromolecules* **1981**, *14*, 1196.
(19) Hashimoto, T.; Shibayama, M.; Kawai, H.; Watanabe, H.; Kotaka, T. *Macromolecules* **1983**, *16*, 361 (part 2 of this series).
(20) Mori, K.; Hasegawa, H.; Hashimoto, T.; Kawai, H., to be submitted to *Macromolecules*.
(21) Skoulios, A. E. In "Block and Graft Copolymers"; Burke, J. J., Weiss, V., Eds.; Syracuse University Press: Syracuse, NY, 1973.
(22) The $D_s$ values of Hashimoto et al.[11] in Figure 2 correspond to the Bragg spacing calculated from the position of the first-order scattering maximum. The spacing is related to the cell edge $a_c$ of the cubic lattice or the interparticle distance $D_0$: $D_s = a_c = D_0$ for sc and $D_s = a_c/2^{1/2} = D_0(2/3)^{1/2}$ for bcc. From the relative peak positions ($1:\sqrt{2}:\sqrt{3}:\sqrt{4}:\sqrt{5}$:...) we know that the spherical domains of our specimens are arranged either in a sc or bcc lattice.[11] However, the volumetric considerations tend to suggest that the sc lattice is more probable than the bcc for bulk structure although some uncertainity still remains unresolved. Thus our $D_s$ values in Figure 2 should be equal to $a_c$ and $D_0$.
(23) This assumption is crude, especially at lower concentrations.
(24) The rigorous value of the exponent ($^1/_3$) also may be affected to some extent by the nonequilibrium effect at the lower concentrations, but we ignore here the small nonequilibrium effect.
(25) Ruland, W. *J. Appl. Crystallogr.* **1971**, *4*, 70.

(26) Hadziioannou, G.; Skoulios, A. *Macromolecules* **1982**, *15*, 258.
(27) Richards, R. W., private communication. Richards, R. W.; Thomason, J. L. *Macromolecules* **1983**, *16*, 982.
(28) Bates, F. S., private communication.
(29) Pedemonte, E.; Turturro, A.; Bianchi, V.; Devetta, P. *Polymer* **1973**, *14*, 145.
(30) Douy, A.; Gallot, B. *Makromol. Chem.* **1981**, *182*, 265.
(31) Richards, R. W.; Thomason, J. L. *Polymer* **1981**, *22*, 581.
(32) Bates, F. S.; Cohen, R. E.; Berney, C. V. *Macromolecules* **1982**, *15*, 589.
(33) Flory, P. J. "Principles of Polymer Chemistry"; Cornell University Press: Ithaca, NY, 1967.
(34) de Gennes, P.-G. "Scaling Concepts in Polymer Physics"; Cornell University Press: Ithaca (NY) and London, 1979.
(35) Vonk, C. G. *J. Appl. Crystallogr.* **1973**, *6*, 81.
(36) LeGrand, D. G. *J. Polym. Sci., Part B* **1970**, *8*, 195.
(37) Kim, H. *Macromolecules* **1972**, *5*, 594.
(38) Hashimoto, T.; Nagatoshi, K.; Todo, A.; Hasegawa, H.; Kawai, H. *Macromolecules* **1974**, *7*, 364.
(39) Bonart, R.; Müller, E. H. *J. Macromol. Sci., Phys.* **1974**, *B10* (1), 177.
(40) Hashimoto, T.; Todo, A.; Itoi, H.; Kawai, H. *Macromolecules* **1977**, *10*, 377.
(41) Todo, A.; Uno, H.; Miyoshi, K.; Hashimoto, T.; Kawai, H. *Polym. Eng. Sci.* **1977**, *17*, 587.
(42) Koberstein, J. T.; Morra, B.; Stein, R. S. *J. Appl. Crystallogr.* **1980**, *13*, 34.
(43) Campos-Lopez, E.; McIntyre, D.; Fetters, L. J. *Macromolecules* **1973**, *6*, 415.
(44) Roe, R.-J. *J. Appl. Crystallogr.* **1982**, *15*, 182.

# Theory of Block Copolymer Micelles in Solution

**Jaan Noolandi* and Kin Ming Hong**

*Xerox Research Centre of Canada, 2480 Dunwin Drive, Mississauga, Ontario, Canada L5L 1J9.* *Received December 13, 1982*

ABSTRACT: A simple model of AB diblock copolymer micelles in solution is presented. A spherical shape is assumed, with a completely uniform inner core formed from the insoluble B blocks and a uniform outer shell composed of the soluble A blocks. The interaction parameters, as well as the molecular weight, composition, and overall volume fraction of the copolymers, are assumed to be given. All energetic and entropic contributions to the free energy can be written down simply, with the exception of the interfacial tension $\gamma$ of the asymmetric interphase. An approximation for $\gamma$ is developed, and the free energy is minimized to obtain the equilibrium size of the micelle. Good agreement with the small-angle X-ray scattering data on the polystyrene/polybutadiene/*n*-heptane system is obtained. Numerical results, as well as scaling arguments, indicate that the size of the micelle, even for different block copolymer compositions, is characterized by power law functions of the total molecular weight of the block copolymer.

## 1. Introduction

Although there is a vast experimental literature on diblock copolymer micelles in selective solvents (ref 1–5 and numerous references contained therein), little theoretical work has been done to predict their structural properties from equilibrium statistical mechanics. In particular, given the overall volume fraction of block copolymer in solution, as well as its molecular weight and chemical composition, one would like to know the sizes of the insoluble core and the soluble outer shell, the degrees of swelling of the two blocks, and the number of polymer chains per micelle. These predictions can then be checked against the results of small-angle X-ray scattering experiments.

In this paper, we present a simple model from which these quantities can be calculated in a straightforward way. We note, however, that we consider only lyophilic systems. Although micellar solutions obtained with amphiphilic block copolymers in the presence of water, oil, and alcohol have been intensively studied recently,[6-10] the corresponding theoretical treatment involves more parameters and will not be discussed here. For the present work, the only complication that arises is the determination of the interfacial tension between the soluble and insoluble blocks of the micelle. We deal with this problem by referring to a general (mean field) expression for the interfacial tension $\gamma$ of an asymmetric interphase derived earlier[11] using the functional integral formalism. For the present situation, we develop an approximation for $\gamma$ that involves only $\chi$ parameters and the (bulk) volume fractions of polymers away from the interphase. The derivation is given in the Appendix.

In section 2, we describe the micelle model in detail. The contributions to the free energy come from polymer–polymer and polymer–solvent interactions, the combinatorial entropy of the solvent molecules, the entropy loss from localization of block copolymer joints at the interphase, the entropy loss from the stretching of the blocks, and the loss of entropy from the turning back of polymers at the interphase. We assume uniform polymer density profiles in both the soluble and insoluble parts of the micelle, and consequently no integrals over the free energy density remain in the final expressions.

The comparison of experiment and theory is discussed in section 3, with the results summarized in Table I. For definiteness, we have chosen a particular set of experiments carried out by Plestil and Baldrian.[2] Section 4 contains the conclusions, with emphasis on the theoretically predicted power law dependencies of the micelle size parameters on molecular weight. Similar results for the power laws only have been obtained earlier by de Gennes,[12] whose work, however, does not allow a prediction of the various size parameters.

## 2. Description of Micelle Model

As described in one of our earlier publications,[13] we assume a spherical model for the micelle, shown in Figure 1, that is made up of three uniform regions. In the presence of a poor solvent for the B block of the copolymer, the center core, labeled as region 1, is composed of a concentrated solution of B chains. The outer shell (region 2) is formed from a less concentrated solution of A blocks of the copolymer. Hence, the solvent–polymer interaction parameter for the A block ($\chi_{AS}$) is assumed to be much smaller than that for the B block ($\chi_{BS}$). The outside of the micelle, region 3, is composed of pure solvent. The radius $l_B$, and the thickness of the shell, $l_A$, are the average

0024-9297/83/2216-1443$01.50/0 